RSC Advances

ROYAL SOCIETY OF CHEMISTRY

www.rsc.org/advances

Cite this: DOI: 10.1039/c0xx00000x

www.rsc.org/xxxxxx

ARTICLE TYPE

Design of Portable Nanosensor for Easy Breast Tomography

Ali Rostami[a], Ahmad SalmanOgli[ab]*, Farshad Farhadnia[a], Mahbobeh Dolatyari[a], Ghassem Rostami[a], and Erhan Piskin[b]

[a]**School of Engineering-Emerging Technologies, University of Tabriz, Tabriz 5166614761, Iran.**

[b]**Hacettepe University, DChemical Engineering Department and Bioengineering and Biyomedtek/Nanobiyomedtek, Ankara Turkey**

In this study, a portable nanosensor for early and easily detection of carcinoma tumor was designed and simulated. The nanosensor consisted of deposited nanoparticles with a regular distance from each other. It has highly sensitivity to the alteration of electromagnetic fields, which are scattered from different tissues (normal and tumor). With respect to the fact that normal tissue permittivity differs from the permittivity of tumors, the interaction of electromagnetic wave with them lead to different results in the case of electrical field and its gradient profile. It means that the non-uniformity will be occurred and this case is a meaningful signal for detection. Nevertheless, it is obvious that, due to tissue absorption coefficient, scattered photons will be very negligible; and a small fraction of the photons reach to the detector. Hence, in this paper, a sensor based on nanoparticles is proposed, which has enough sensitivity to pick up scattered photons, amplify, and detect them. It should be noted that, the roles of the nanosensor between body surface and detector are the signal amplification and sampling via nanoparticle plasmonic effect. It means that the designed nanoparticles sample the scattered waves and amplify them in the near-field. At last, our design and simulation results show that the digitized signals could be easily and clearly detected by force or temperature detectors. So, the easy breast tomography will be carried out with no need to clinics and its equipment.

Introduction

The obvious regretful fact is that cancer is the second leading cause of death in the world; researchers have done their best to find purely safe treatments for cancer. The development of nanobiotechnology and nanomedicine is considered to be among the most promising advances in cancer treatment. It refers to the application of small materials and devices whose sizes are measured in the billionths of a meter to detect, diagnose, and treat cancer and other disease by modern approaches [1-4]. When compared with other available common therapies [5-7] such as chemotherapy, radiotherapy and surgery, nanomedicine has proven to be especially promising in fighting cancer. Drug delivery is the most important case with high accuracy rather than common methods in the treatment of cancer. So, it must be regulated with high precision targeting and imaging. It has been proven that the main disadvantages of common methods such as chemotherapy are related to use of non-targeted drugs for killing cancerous tumor. However, it should be maintained that in the field of nanotechnology and nanomedicine, the accurate detection of tumor or cancer cells has been carried out by means of effective methods such as active targeting. One of the important features of active targeting is that several biological agents can be attached to the surface of nanoparticles (NPs) to construct multi-function sensors and simultaneously do several tasks [1-3], [8-11]. It has been investigated that nanomedicine and nanobiotechnology have enormous advantages but they are not regarded as user-friendly and easily methods. Moreover, they must use in clinical tries. Thus, nowadays, researchers aspire to find user-friendly methods which have the advantage of earlier detection. In this paper, a method has been proposed which can perform tumor tomography (especially for breast cancer) with and without active targeting agents. This method works based on the interaction of light (near- and far- infrared frequencies) with different tissues (normal tissue and tumor). In this method, scattered photons are detected by a sensor with a high sensitivity. It is obvious that absorption in a real tissue is too high and the reached photons to the detector are very negligible. Also, the wavelengths of 833, 1550, and 6199 *nm* were used in which the absorption rate in the tissue component matters such as H_2O, *Oxy-* and *deoxy hemoglobin* is low; however, the scattered photons are small. Hence, for solving this problem, a sensor with

high sensitivity which has no extra noise should be designed to detect photons. In this study, such a sensor was designed based on core/shell NPs which was intended to detect and manipulate the small fraction of scattered photons. Simulation results show that the order of photons in critical conditions is about of 0.1 W/cm^2. Therefore, to sort out this critical issue, photon amplification by NPs in the near-field state was used. That is to say, when a light interacts with NPs, all the carriers on the NPs surface harmoniously resonance. This case which has contributed to the NPs plasmonic resonance leads to high intensity and non-uniform electric field in the closeness of NPs [12-14]. In other words, NPs resonance in the plasmonic state can amplify the reached signals and detect them in the near-field state. Moreover, the plasmonic-plasmonic interaction between NPs can intensify the gradient of the electrical field and, hence, the detected photons will be improved. In the following, the mathematics and theoretical section of work are presented. Furthermore, the theoretical and simulation operations were conducted by MATLAB and COMSOL, respectively.

Mathematics and Theory

Penetration of light in tissue

Light propagation in tissue is an important question in different biological applications such as imaging, sensing, and targeting. Numerous methods, including analytical, numerical and statistical ones have been developed for predicting light propagation in tissue [17]. Optical parameters are obtained by use of measured parameters such as reflection, transmission, and absorption and converting them into parameters which characterize light propagation in tissue. It has been reported that most of the advances regarding laser light transfer in tissues are based on transport theory [17-18]. It should be noticed that the superiority of this theory in tissue optics to many analytic methods is attributed to the non-homogeneity of biological tissues. Transport coefficients can be derived from the collision of a plane wave with a particle; thus, some of the waves are absorbed, some are scattered and some of them are unperturbed and transmitted. It seems that the transport equation is one of the complete methods for defining tissue optical parameters and light propagation in tissue. The radiative transport equation is given by:

$$(\mu_a+\mu_s)L(r,s)+(\mu_s/4\pi).\int_{4\pi} p(s,s').L(r,s')d\Omega \quad (1)$$

Where $L(r,s)$ refers to the radiance at position r in the direction of vector s and $d\Omega$ denotes differential solid angle. The parameters μ_a and μ_s indicate the medium absorption and scattering coefficients, respectively. The phase function $p(s,s')$ represents the fraction of scattered light from direction s' into s. In this study, delta-Eddington phase function is used as the phase function which is given by:

$$P_{delta-Eddington}(\cos\theta)=(1/4\pi).\{2f\,\delta(1-\cos\theta)+(1-f).(1+3g'.\cos\theta)\} \quad (2)$$

Where $\cos(\theta)=(s.s')$ denotes the cosine angle between the incident and the scattered light. The first term indicates strong scattering in the forward direction and the second term contributes to diffuse scattering. Moreover, the parameters f and g' are the fraction of light in the forward direction and the degree of asymmetry in the diffuse section, respectively.

Substituting Eq. 2 into Eq. 1 yields:

$$(s.\nabla)L(r,s)=-(\mu_t')L(r,s)+(\mu_s/4\pi).\int_{4\pi}(1+3g'(s,s'))L(r,s')d\Omega \quad (3)$$

Where $\mu_{t'}=\mu_a+(1-f).\mu_s$ is the transport coefficient and is less than $\mu_t=\mu_a+\mu_s$; this is due to the fact that the fraction of light is scattered to the s direction from s'. Moreover, the reduced scattering coefficient can be defined as $\mu_{s'}=(1-f).\mu_s$

The radiance is divided into collimated and diffuse components:

$$L(r,s)=L_{col}(r,s)+L_d(r,s) \quad (4)$$

The collimated radiance includes both the light scattered into direction parallel to the incident beam and any un-scattered light which is represented as:

$$L_{col}(r,s)=(1-r_s).\pi F_0(r).\exp(-\mu_t' z/\mu_0).\delta(\mu-\mu_0) \quad (5)$$

In this equation, r_s is the specular reflection coefficient given by Fresnel reflection formula. F_0 is the initial irradiance and μ is angle between s and z and $\mu_0 = s*z$. By substituting Eq. 5 into Eq. 4 and simplifying it, we will have the following:

$$(s.\nabla)L_d(r,s)=-(\mu_t').L_d(r,s)+\{(\mu_s'/4\pi).\int_{4\pi}(1+3g'(s,s')).L_d(r,s')d\Omega\} \quad (6)$$
$$+\{(1-r_s).\pi F_0(r).\exp(-\mu_t' z/\mu_0).(\mu_s'/4\pi).(1+3g'.\mu/\mu_0)\}$$

For further simplification, the diffuse radiance can be written as:

$$L_d(r,s)=(1/4\pi).\varphi_d(r)+(3/4\pi).F_d(r).s \quad (7)$$

Where φ_d and F_d represent the isotropic and anisotropic contribution to the diffuse radiance, respectively. Finally, by substituting Eq. 7 into Eq. 6 and further simplifying, the diffuse radiance is represented as the following:

$$(s.\nabla)\varphi_d(r)+3(s.\nabla)(F_d(r).s)=-(\mu_a)\varphi_d(r)-3(\mu_t'-g\,\mu_s')(F_d(r).s) \quad (8)$$
$$+\{(1-r_s).\pi F_0(r).\exp(-\mu_t' z/\mu_0).(\mu_s'/4\pi).(1+3g'.\mu/\mu_0)\}$$

Eq. 8 contains isotropic and anisotropic diffuse form. For solving this equation, one of them could be written based on the other, which leads to the following Helmholtz equation:

$$\nabla^2\varphi_d(r)-3\mu_{tr}'\mu_a\varphi_d(r)=-3\{\mu_s'(1-r_s).\pi F_0(r). \quad (9)$$
$$\exp(-\mu_t' z/\mu_0).(\mu_{tr}+g'.\mu_s')\}$$

This equation is solved based on diverse boundary conditions at the interface between two media. Then, by solving this equation, the radiances at different points of simulation area as well as nanosensor surface position are determined. Indeed, the goal of this section is the propagation of the light with different wavelengths into tissue, which is calculated by considering of the medium absorption and scattering coefficients. Finally, in this study, the optical properties of a real tissue were used from experimental results such as the *in vitro* and *in vivo* data [17].

Electric field gradient and optical force

When an electromagnetic wave interacts with NPs, the Δp_{photon} is transferred; then, based on momentum conservation, the particle undergoes an equal and opposite momentum change by $-\Delta p_{photon}$. This momentum change exerts a force on the particle which is given by the change rate of the particle momentum. Two types of forces arise at the interface due to the light-matter interaction. First, one is the scattering force (F_{sca}) which acts along the direction of light propagation and the second one is the gradient force (F_{grad}) which pulls the particle towards the higher intensity region. However, it should be noted that the optical force is raised in a non-uniform electric field and it will be disappeared in a uniform field. Since tissue and tumor have different interactions with light, the non-uniform electric field is caused in the medium by inhomogeneity in the medium. Nevertheless, it should be

pointed out that nanosensor output non-uniformity is produced due to the plasmonic resonance of NPs. That is, at the closeness of any deposited NPs, non-uniformity is created which is related to the interaction of the scattered light with NPs. Hence, due to the non-uniformity of NPs which is distributed in the nanosensor output, its measurable parameter such as optical force could be analyzed. For better investigation, the optical force has been theoretically discussed in this section. It has been reported that the time-average force on a dipole in harmonic electromagnetic field can be defined as [15, 16]:

$$\langle F \rangle = (1/4).\mathrm{Re}(\alpha).\nabla |E|^2 + (\kappa/2).\mathrm{Im}(\alpha).\mathrm{Re}(E^* \times B) + (1/2).\mathrm{Im}(\alpha).\mathrm{Im}[(E^* \nabla).E] \quad (10)$$

Where F, α, E, B, and κ denote optical force, polarizability, electrical field, magnetic field, and wave vector, respectively. In this equation, the first term on the right is gradient force and the next terms were cooperatively titled as the scattering force. For proving Eq. 10, the researchers began with an expression for negative gradient of the classical dipole-field interaction Hamiltonian:

$$\langle F \rangle = (1/2).\sum e_i.\mathrm{Re}[\alpha.E.(\partial E/\partial x_i)^*] \quad (11)$$

where i,e_i refer to the Cartesian component and the related normal vector, respectively. By simplifying Equation 11, the following is obtained:

$$\langle F \rangle = \sum e_i.\mathrm{Re}(\alpha)(\partial |E|^2/\partial x_i) + (1/2)\sum e_i.\mathrm{Im}(\alpha).\mathrm{Im}[E^*.(\partial E/\partial x_i)] \quad (12)$$

In this equation, the first term is related to gradient force and the second one is related to the scattering force. Previous studies and investigations have indicated that as a result of manipulating core/shell NPs, the magnitudes of gradient force is far greater than that of scattering force and the aforementioned case can be negligible [13]. Hence, in this study, the gradient force is calculated and referred to optical force.

Nanoparticles local temperature

When an electromagnetic wave interacts with any NPs, the optically stimulated NPs generate heat. In other words, NPs can effectively produce heat under light irradiance. The mechanism of heat generation by NPs is very simple; the electromagnetic field strongly derives mobile carriers into the NPs and the energy gained by carriers turns into heat. Then, the heat diffuses away from the NPs and leads to an increase in the local temperature around them. It should be noted that the heat released by NPs becomes strong in the case of plasmonic resonance in the metal NPs. The occurrence of plasmonic resonance depends on NPs size, materials, shape, electromagnetic wavelength, and medium dielectric constant. In this paper, multi-shell NPs with different materials were used. Hence by changing core and shell sizes, the plasmonic resonance (magnitude and peak wavelength) will be altered. Moreover, in the core/shell structure, the plasmonic-plasmonic interactions could be raised. In other words, the plasmonic in the core and outer shell will interact with each other; this interaction can manipulate the electric and current density in the structure. So, the magnitude of energy gained by mobile carriers is altered. Under this condition, the temperature distribution around NPs is given by the heat transfer equation [20, 21]:

$$\rho(r).c(r).\partial T(r,t)/\partial t = \nabla\kappa(r).\nabla T(r,t) + Q(r,t) \quad (13)$$

Where r, t, $T(r,t)$, $p(r)$, $c(r)$, and $\kappa(r)$ denote the coordinate, time, local temperature, mass density, specific heat, and thermal conductivity, respectively. $Q(r,t)$ represents an energy source from wave dissipation in NPs and is obtained through the following equation:

$$Q(r,t) = \langle j(r,t).E(r,t) \rangle_t \quad (14)$$

Where $j(r,t)$ and $E(r,t)$ denote the current density and electric field in the system, respectively. For solving of the Eq. 13, several numerical and analytical methods have been commonly used. It is notable that in this work, time variant section of temperature is not important and can be neglected, so we solved the temperature equation in the steady-state condition. With substituting Eq. 14 into Eq. 13 and solving it in the steady-state condition, the local temperature around any NPs is described by this equation [20]:

$$\Delta T(r) = V_{NPs}.Q(r)/4\pi.\kappa_0.r \quad (15)$$

Where r, κ_0, and V_{NP} refer to the NPs radius, the thermal conductivity of surrounding medium, and NPs volume, respectively. Moreover, $Q(r)$ represents an energy source from wave dissipation in NPs. It is severely raised due to interaction of light with NPs at which the NPs resonate in the plasmonic state. In the other word, by controlling of the plasmonic key parameters, the heat generation by NPs will be changed. Based on the above-mentioned equations, it can be pointed out that the heat generation rate and temperature enhancement depend on the physical properties of material. It has been indicated that the heat generation efficiency by Au NPs is about 10^{-3} under the plasmonic resonance conditions [20]. Nevertheless, it should be mentioned that this efficiency can be optimized by plasmonic hybridization in the core/shell NPs. Moreover, heat generation by NPs can be dramatically enhanced in the presence of several NPs. This is contributed to the interaction mechanism between NPs, namely accumulative effect and Coulomb interaction. The accumulative effect refers to the addition of heat fluxes produced by the NPs. However, in the case of Coulomb interaction, the generated heat is affected by the interaction of neighboring NPs and the total amount of generated heat by the two interacting NPs will be different from the amount of produced heat by two single NPs; this is attributed to the partial screening of electric field inside the NPs. Also, this effect may come from the shift of plasmon resonance which results from NPs Columbic interaction. With respect to the recent use of the NPs Columbic interactions for enhancing heat generation, the plasmonic-plasmonic interactions between adjacent NPs were used in the present study to enhance temperature signal. In the following, the nanosensor structure designing and simulation results about light propagation in a real tissue and output signal sampling by NPs are presented, respectively.

Nanosensor structure

In this study, the designed sensor is based on the deposition of core/shell NPs in the defined distance from each other. The *3-D* and *2-D* illustrations of this sensor are depicted in the left and right sides of figure 1, respectively. This schematic shows that the nanosensor covers the whole breast and the electromagnetic or

laser source is placed on top of it. The size of the smallest element of nanosensor (pixel) is about 10.2 *um* and it includes an *N*M* NPs matrix in which *N* and *M* are matrix incidences. It should be mentioned that in this work, NPs with a core and two shells such as *Au/SiO$_2$/Au* were used. Step-by-step of multi-shell NPs forming process and moreover their optical characterization has been reported in [12]. In this reference, it is seen that the experimental and theoretical characterizations of *Au/SiO2/Au* NPs are interestingly fitted to each other and easily manipulated by changing of NPs geometry. The gap between core and outer shell is made of dielectric materials since the NPs plasmonic hybridization, as an important parameter, is manipulated. Another important parameter in the design of the nanosensor was the medium materials in which the NPs were inserted; this is due to the fact that the medium material thermal conductivity and its dielectric constant have an impact on nanosensor outputs. The *aerogel silica* or *silica* was used as the medium materials in this study. In most simulations, the *aerogel silica* was used instead of *silica* due to its controllable thermal conductivity and dielectric constant. Moreover, the NPs outer shell size radius was approximately considered 150 *nm*. The inner shell and core radius were altered to improve nanosensor output, which is related to the hybridization of plasmonic in the core and outer shell. Furthermore, for the incidence of laser light on matter, three wavelengths as 833 *nm*, 1550 *nm*, and 6199 *nm* were used. Finally, the two distinct phenomena including optical force and thermal effect could be sensed by piezoelectric detectors [25, 26]. For practically fabrication of the portable nanosensor, which is schematically illustrated in fig. 1, nanoreplica molding process can be used. This process has been demonstrated as a low cost and suitable method for manufacturing periodic NPs based structures. It is notable that this method is performed using low force at room temperature to create nanometer-scale structures with high uniformity, which is very important in our work, over a large area using a patterned silicon wafer as a reusable molding template [27].

Discussion

The high efficiency nanotechnology-based method has been recently introduced to detect carcinoma tumors. This method is based on active targeting in which the functionalized NPs are injected to the body. Thanks to their attached elements such as proteins, enzymes, and antibody, the functionalized NPs are considered to be smart agents. They can precisely find a target and accumulate to its nearby location. After the accomplishment of targeting by the smart NPs, the effective therapy will be fulfilled by the drug delivery. However, in general, it should be maintained that this approach is not effective since it cannot be used easily and it calls for clinical equipment. Nevertheless, in the present study, a new approach has been proposed which is able to portably detect the breast cancer tumor independently of any injected agents. Also, the test can be accomplished without need to anyone or clinics. This method is based on the interaction of light or an electromagnetic wave with the breast tissue in which the detection of scattered photons is carried out by a very sensitive sensor. It has been proven that the dielectric constant and permittivity of the normal and abnormal cells are different from each other [22, 23]. That is, the optical properties of carcinoma and normal cells are different and the amount of photon scattering and absorption are different for two distinct tissues (normal tissue and tumor). In other word, when a tumor initially starts to be constructed, the dense matter of the tissue with abnormal state is replaced by a normal tissue. In its construction mode, the electrical properties of the tissue such as permittivity, conductivity, and so on is altered which is attributed to the new blood vascularization and proliferation rate in the tumor medium. Thus, the interaction of light flux with the normal and abnormal tissue results in different profiles of electrical field and its gradient in the output, which is related to an enormous non-uniformity. So, it was easy to detect the field non-uniformities by some different practical methods. Nevertheless, an important drawback of this method is too absorption of light in tissue which limits the penetration of light into tissue. For solving this problem, two approaches were used in this study: I. Wavelength selection in which the minimum light is absorbed into tissue (for minimizing tissue loss, three different wavelengths 833, 1550, and 6199 *nm* were used at which the absorption of H_2O and *oxy-* and *deoxy-hemoglobin* are small); II. The improving of the nanosensor specification. The latter case is carried out based on NPs plasmonic resonance and plasmonic hybridization which produces high intensity field and field gradient near the NPs. In the following sections, a detailed and step-by-step description of the proposed method is given. Figure 2 illustrates the proposed method. In this, the arrangement of nanosensor, detector, core/shell NPs, pixels of nanosensor and a pixel of detector are schematically depicted. As shown in this schematic, when electromagnetic wave with definite wavelength (833, 1550, or 6199 *nm*) is radiated on the breast area, most incident photons will be absorbed in the tissues with respect to their absorption coefficient and a few photons will be scattered which can be detected by the nanosensor. Moreover, piezoelectric and nanosensor typical data for design are reported in this schematic. It should be noted that the simulated piezoelectric detector like to reported case in [25] could sense a force about 1 μN. In the following of simulation, at first, the propagation of light into a tissue was simulated by solving Helmholtz equation. Simulation results indicate that the photons detected by nanosensor were very small and were not easily recorded where the detected ones were disturbed by background noise.

However, it should be considered that the photons scattered from distinct tissues were different which is related to their optical properties. It means that, when an electromagnetic wave interacts with different matters which have distinct optical properties (scattering, absorption, and anisotropy), the reached scattered photons in the sensors from different tissues construct a tangible profile after photons amplification by NPs. So, in this study, the nanosensor was designed to detect a small fraction of scattered photons, amplified them in the near-filed and finally above all, sampling the continuous output signals. The latter case is the most important result in the clearly detection of output, which is contributed to the NPs plasmonic resonance. It should be noted that the continuous and attenuated signal detection is very hard due to distortion by several noises. Indeed, the sampling rate is controlled by manipulating of NPs distance from each other and their plasmonic-plasmonic interactions, which surely influence on

signal detection. At last, the digitized signals are scanned by detectors to construct the field and its gradient profile based on variety of tissues. In other words, the nanosensor output signal is sampled by NPs plasmonic which is easily controllable. Indeed, output signal sampling refers to the use of NPs plasmonic in the near-field state. For this, the core and shell plasmonics interact with each other with different strength which depends on the distance between core and outer shell. The plasmonic interaction inside the NPs has a strong effect on the optical force and local temperature around NPs, which are used to detect the scattered photons. The optical force is related to the electrical field gradient and the NPs local temperature depends on the electrical field and current density. Moreover, in the design of nanosensor, the Coulomb interaction of NPs was used to improve the heat generated by NPs. It should be pointed out that the Coulomb interaction between NPs might have an impact on partial screening of the electric field inside the NPs. Thus, this case can have a dramatic impact on the NPs plasmonic resonance. High sensitivity of a nanosensor severely depends on the NPs interactions which are determined by the distance of NPs from each other in the nanosensor. With regard to this issue, the designed nanosensor can detect the small variation of tissues as the optical properties change. In the following section, the simulation results in the case of detecting tumor inside the tissue are illustrated and perused.

Results

In this section, the simulation results including light propagation in a typical tissue at different wavelengths and nanosensor outputs are discussed. Initially due to the significance of light propagation into a tissue, the light penetration into Murine albino is investigated. Table 1 shows the tissue optical properties at different wavelengths. By incidence of light with angle=0 *rad*, a minimum photon lost will be occurred, which is due to tissue surface light reflection with regard to Fresnel's law. Figure 3a illustrates that as the wavelength increases, the penetration depth of light into tissue will dramatically increase. The alteration of diffusion flux into tissue regarding non-zero incidence angle is illustrated in figure 3b. This figure illustrates that the penetration of light is severely limited, as the incidence angle is increased. Thus, by selecting a suitable wavelength and incident angle, the magnitude of reached photons on the sensor surface will be controllable. Nevertheless, the absorbed photons in a real tissue are so high. Therefore, the designed sensor should be able to detect a small fraction of light.

In the following section, the important output signals, which are finally related to the optical force and temperature (electrical gradient and total power dissipation), will be discussed. It should be maintained that for investigating the interaction of an electromagnetic wave with a matter, the matter dielectric constant will be needed. At first, the ideal state is simulated in which the data of dielectric constants are used from table 2. In the ideal case, it was assumed that the imaginary part of tissue dielectric constant which is related to the photons absorptions rate is small. Due to its ideal state, the light deeply penetration is occurred into the tissue. The interaction results are illustrated in figure 4. The purpose of these simulations were to compare signal detections before (figures 4a and d) and after (figures 4b and e) the use of nanosensor. It is clearly observed that before nanosensor, the signal is continuous and its resolutions are very low. Therefore, the detection of original signal is so hard by considering of the auto-fluorescence photon radiations. In the case of electric field gradient, illustrated in figure 4d, the non-uniformity is produced, which is due to distinct interaction of matters with light. However, it is limited to the continuity and sharp alteration. In contrast, the signal clarity in the nanosensor output increases which are attributed to the NPs plasmonic resonance effect on signals. In other word, the output signals are sampled by NPs, which their distance and amplitudes are easily manipulated. Indeed, the output signal digitization was the main purpose of this study in which help to detect the output signal with a high resolution. The *2-D* illustration of dissipation power energy and electric gradient field are depicted in figures 4c and 4f, respectively. In these figures, the signal digitization by the NPs plasmonic effect is easily observable. Due to different interactions of light with distinct materials, the non-uniform profile is illustrated in all figures. The non-uniformity at the output of nanosensor dramatically increases which will be detected by detectors. It should be noted that the plasmonic enhanced in the portable nanosensor (for instance, we can consider the results of figs. 4c, 4f), which contains arrays of regulated and patterned multi-shell NPs, is comparable with surface-enhanced Raman nanodomes [27], plasmonic nanogalaxies [28], and surface enhancing by Au NPs [29] results, which contain some theoretical-experimental works in this field but with different applications. In the referred works, the experimental data for enhancing by NPs plasmonics resonance have been reported to be an order of 10^6-10^7-fold. In the following, we will explore the original results of our works, which are related to the detection of non-uniform field created by different tissues. In the real medium, the penetration of light into tissue is limited and very small fraction of light can reach the detector. For this, the data from table 3 are considered. In this case, the imaginary part of the tissue is supposed to be larger than the ideal one. Thus, the majority of photon flux density is absorbed into tissues and only a little density of them, i.e. about 1000 w/m^2 reach the detector. Therefore, we are trying to design a nanosensor which is able to detect a small fraction of the scattered light. The nanosensor was designed by manipulating some parameters such as NPs materials (core, shell_I, and shell_II), NPs radius, core-shell plasmonic hybridization, medium material and irradiance wavelength. Nanosensor output signals which are detected as temperatures or optical forces are illustrated in figures 5 and 6, respectively. All subfigures in figure 5 indicate that the digitized non-uniformity in temperature profiles is related to the interaction of light with different matters and the NPs plasmonic effect. In other word, when the continuum non-uniform field interacts with NPs, the photons are amplified and regularly sampled which are due to NPs plasmonic resonance. Thus, the amplified and digitized signal can be easily measured. Figure 5a depicts temperature profile for tissue dielectric constants from table 3. It illustrates that the fraction of light absorbed into the tissue is too high in the non-ideal state and consequently the temperature will be low. So, in the following, the alteration of nanosensor parameter effects on total dissipation power and temperature are investigated. It should be noted that

other parts of figure 5 are related to the manipulation of parameters, i.e. either nanosensor parameters or tissues optical properties. As shown in figure 5b, the absorption rate of tumor increases which is related to tumor construction area and its physiological condition (neoplasia in tumor [4, 25]). This figure shows that the temperature difference between normal and abnormal tissue increases rather than figure 5a. In other words, the majority of photons in the tumor area are absorbed which leads to a sever non-uniformity. Moreover, the increase in the tumor dielectric imaginary part might be related to the active targeting by functionalized NPs. In active targeting, a large amount of functionalized NPs find the tumor and accumulate in its nearby, which results in the increased absorption rate in this region. Furthermore, as illustrated in figure 3a, the NPs plasmonic act as a photon amplifier and sampler of the received signals. The incidence wavelength effect on light propagation in the tissue and output signal is illustrated in figure 5c. It can be easily observed that the temperature magnitude increases which is not observed in the earlier figures; this is attributed to the increase in the received photon flux on nanosensor surface in the higher wavelength. The effect of NPs distance with each other on output is illustrated in figure 5d. When NPs distances from each other increase, the NPs plasmonic-plasmonic interaction will be decreased. Hence, the sole effect of NPs plasmonic detector screen can be considered. Based on its results, it is considered as an appropriate case for designing nanosensor. In another case, the simultaneous effect of increasing tumor absorption rate and incidence wavelength was investigated and its results are illustrated in figure 5e. In this case, the large amount of light propagation at 1550 *nm* and sever non-uniformity due to tumor absorption coefficient are realized and their influence on total power dissipation is easily observed. In figure 5f, the concurrent effect of incidence wavelength at 6199 *nm* and NPs distance increasing from each other is perused. In this figure, the digitization isn't fully done by NPs, which is contributed to the excitation wavelength at 6199 *nm*. It is right that the penetration of light is severely increased by increasing of wavelength, but this wavelength is far-away from the NPs plasmonic resonance and so, NPs carriers don't effectively resonate in this wavelength. This is contributed to the photoelectric effect in the case of interaction of an electromagnetic wave with NPs. In the following, the effect of medium materials and NPs core and second shell materials were simulated which is depicted in figure 5g, and h, respectively. It can be obviously observed that the use of *SiO2* rather than silica aerogel results in a decrease in the temperature since the *silica* thermal conductivity is bigger than *silica aerogel*. The following simulation is related to the nanosensor changing parameters effect on optical force as another measurable signal of detector. Similar to figure 5, all the subfigures in figure 6 indicate that the sampled non-uniformity in optical force profile is related to the interaction of light with different matters and NPs plasmonic effect. Figure 6a depicts optical force in the non-ideal state. It should be noted that the optical force is directly related to the electric field gradient in the medium. Hence, the non-uniformity of electric field gradient directly affects the optical force. The alteration of tumor absorption coefficient, incidence wavelength, NPs distance from each other, medium and core/shell materials have severe impacts on electrical field non-uniformity and its magnitude. Therefore, it should be maintained that changing electrical field non-uniformity and its magnitude will dramatically affect the optical force profile which are illustrated in figures 6b, c, d, e, f, g, and h, respectively. These figures reveal that the magnitudes of optical force, due to NPs plasmonic effect, are in the order of μN which can be easily measured by piezoelectric detectors [25, 26]. Indeed, the detector senses the distinct forces due to the difference in tissues which is related to non-uniformity in detected signals. It can be easily noted that the signals are digitized by NPs which cause lightly its measure. The maximum optical force, shown in figure 6h, is due to the alteration of medium materials. Figures 5 and 6 reveal that the NPs plasmonic remarkably affect temperature and optical force. That is to say, NPs plasmonic resonance manipulates the total dissipation energy and electric field non-uniformity near field state and leads to photons amplification. Furthermore, the tumor active targeting by functionalized NPs influence was investigated in the present study, which is shown in figure 6e. At last, the simulation results claims that the output sampled signals could be easily and clearly detected by force and temperature detectors. So, the easy breast tomography will be carried out with no need to clinics and its equipment.

Conclusions

In this study, a portable nanosensor for the early and easily detection of a carcinoma breast cancer was designed and simulated. Based on theoretical simulations, it was indicated that the backscattered photons reached to the sensor surface were very small and were significantly affected by background noises. Hence, it is very hard to detect them without any photon intensification. Moreover, the interaction of the incidence light with a matter with different optical properties cause to electrical field non-uniformity, which should be detected. For this, the NPs based sensor in which the NPs plasmonic resonance causes to the signal amplification and digitization, is employed. It is notable that the original drawback of earlier works, which was related to the unclear and attenuated signals on the detector, is improved by NPs plasmonic influence. In other words, the received photons on nanosensor surface are sampled and amplified by NPs, which leads to easily detection of much attenuated signals. So, the digitized signal is easily filtered and controlled for other signal processing. Finally, the easy breast tomography will be carried out with no need to clinics and its equipment.

Acknowledgements: This study is partially supported by photonic group of school of engineering-emerging technologies, University of Tabriz and moreover is partially supported by EU-FP7-IAPP NanobacterphageSERS and Biyomedtek/Nanobiyomedtek. A. Salmanogli was supported by this project as a recruited fellow. E.Piskin was supported as member of Turkish Academy of Sciences (TUBA).

Notes and references

Fax: +98-0411-3377887, a.salmanogli@tabrizu.ac.ir

1 A. Name, B. Name and C. Name, *Journal Title*, 2000, **35**, 3523;
1 N. Paras, *Multimodal Imaging*, NCI Reports, 2010.
2 G. Lanza, *New Contrast Agents with Improved Spatial and Temporal Resolution*, NCI Reports, 2010.
3 Sh. Nie, *Nanotechnology for Image Guided Interventions*, NCI Reports, 2010.
4 R.A. Gatenby, R.J. Gillies, *Nature Reviews Cancer*, 2004**, 4,** 891.
5 M. Kara Bucci, A. Bevan, M. Roach, *CA Cancer J Clin***,** 2005**, 55,** 117.
6 K. L. Kimberly, K. Christine, F. R. William, *Obstet Gynecol Clin N Am*, 2005, **32,** 627.
7 A. E. OMOTI, C. E. OMOTI, *Pharmacy Practice*, 2006, **4,** 55.
8 P. F. Jiao, H. Y. Zhou, L. X. Chen, B. Yan, *Current Medicinal Chemistry*, 2011, **18,** 2086.
9 A. SalmanOgli, *Cancer Nano*,2011, **2,** 1.
10 G. von Maltzahn, Ji-Ho. Park, K. Y. Lin, N.Singh, Ch. Schwöppe, R. Mesters, W. E. Berdel, E. Ruoslahti, M. J. Sailor, S. N. Bhatia, *NATURE MATERIALS j*,2011, **10,** 545.
11 B. Van de Broek, N. Devoogdt, A. D'Hollander, H. L. Gijs, K. Jans, L. Lagae, S. Muyldermans, G. Maes, G. Borghs, *ACS NANO*, 2011, **5,** 4319.
12 R. Bardhan, *Nanostructures for Plasmon Enhanced Fluorescence Sensing: From Photophysics to Biomedicine*, PhD thesis, HOUSTON, TEXAS University, 2010.
13 A. SalmanOgli, A. Rostami, *IEEE transaction on Nanotechnology*,2013, **12,** 12, 831.
14 A. SalmanOgli, A. Rostami, *IEEE transaction on Nanotechnology*,2013, **12,** 558.
15 V. Wong, M. A. Ratner, *Physical Review B*,2006, **73,** 075416.
16 A. SalmanOgli, A. Rostami, M. Faranoush, M. dolatyari, G. Rostami, *RSC Adv.*2014, **4,** 30984.
17 W. Cheong, S. A. Prahl, A. J. Welch, *IEEE journal of Quantum Electronics*, 1990, **26,** 2166.
18 J. H. Joseph, W. J. Winsombe, *Journal of the Atmospheric Science,* 1976, **33,** 2452.
19 H. Ding, J. Q. Lu, W. A. Wooden, P. J. Kragel, Xin-Hua. Hu, *Phys. Med. Biol*, 2006, **51**, 1479.
20 A. O. Govorov, H. H. Richardson, *nanotoday*, 2007, **2,** 2, 30.
21 A. SalmanOgli, A. Rostami, *IEEE transaction on Nanotechnology*, 2012, **11,** 1183.
22 S. Haltiwanger, *The Electrical Properties of Cancer Cells*, http://www.royalrife.com/haltiwanger1.pdf.
23 B. RO, *Medical Times*, 1976, **95,** 95, 657.
24 Y. Jiang, J. P. Grbovic, C. Y. Cantrell, J. P. Freyer, *Bio physical Journal*, 2005, **89,** 3884.
25 J. Xu, M. J. Dapino, D. Gallego-Perez, D. Hansford, *Sensors and Actuators A*, 2009, **153,** 24.
26 N. Ferrell, J. Woodard, D. J. Hansford, *Sensors and Actuators A*, 2011, **170,** 84.
27 Ch. J. Choi, Zh. Xu, H. Yu. Wu, G. L. Liu and B. T. Cunningham, *Nanotechnology*, 2010, **21**, 415301.
28 Zh. Zhang, P. Yang, H. Xu, and H. Zheng, *Journal of Applied Physics*, 2013, **113**, 033102.
29 A. Gopinath, S. V. Boriskina, W. R. Premasiri, L. Ziegler, B. M. Reinhard, and L. Dal Negro, *Nano Letters*, 2009, **9**, 3922.

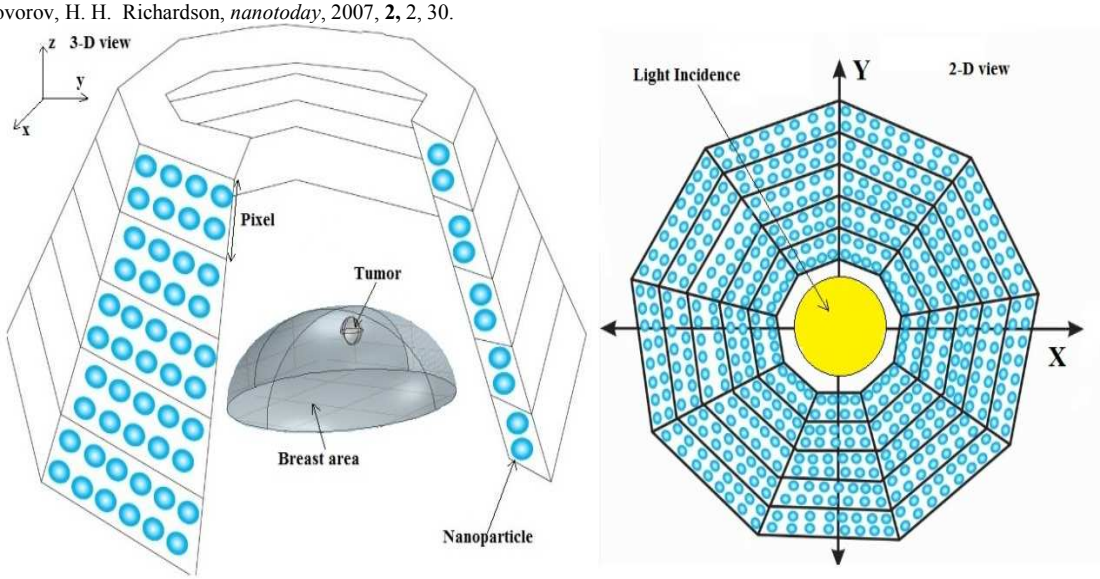

Figure. 1 3-D and 2-D illustration of nanosensor, NPs arrangement in each pixels, Laser incidence in the z- coordinate, and schematic of breast covering by nanosensor

Table 1. Tissue: Murine (albino) Optical properties vs. wavelengths [17, 18]

	488 nm	800 nm	1064 nm	1320 nm
Absorption coefficient (μ_a) (1/cm)	12.2	5.7	5.9	6.1
Scattering coefficient (μ_s) (1/cm)	173.5	97	60.9	44.2
Anisotropy factor (g)	0.93	0.94	0.92	0.91

Table 2. Initial properties of tissue dielectric constant and nanosensor specification (ideal state); ntumor is approximated based on normal tissue.

n_{tissue} [19]	1.37+i0.016
n_{tumor}	1.37+i0.16
wavelength	833 *nm*
NPs_material (core and shell_II)	Au
Medium_material	Silica Aerogel
NPs_material (shell_I)	SiO_2

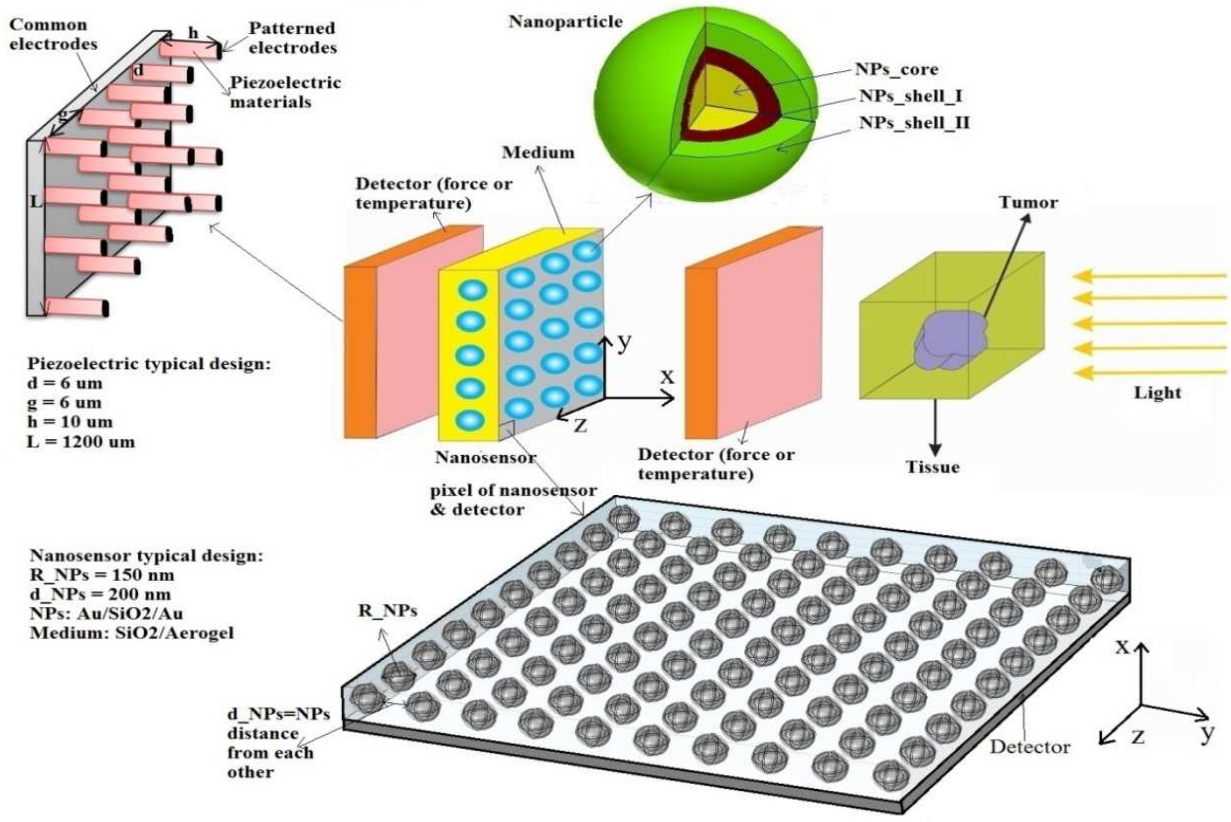

Figure. 2 illustrations of framework; Irradiance of light (w/cm^2.sr) in the x-coordinate and measuring of optical force or temperature by detectors in the y- and z- coordinates and zoom out of nanosensor's and detector's pixel.

Table 3. General properties of tissue dielectric constant and nanosensor specification (non-ideal state)

n_{tissue}	1.37+i0.16
n_{tumor}	1.37+i0.5
wavelength	833 *nm*
NPs_material (core and shell_II)	Au
Medium_material	Silica Aerogel
NPs_material (shell_I)	SiO_2

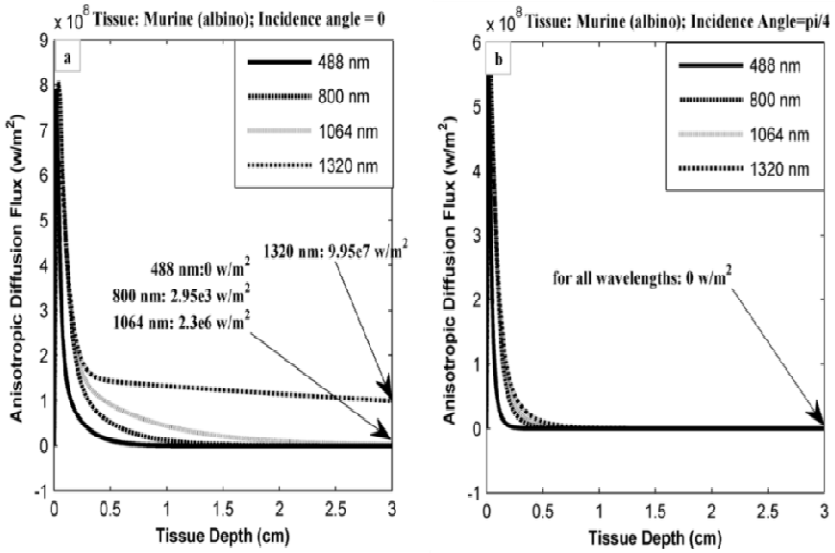

Figure. 3 Anisotropic diffusion flux (w/m^2) vs. tissue depth (cm); a) Irradiance angle = 0 rad, b) Irradiance angle = pi/4 rad

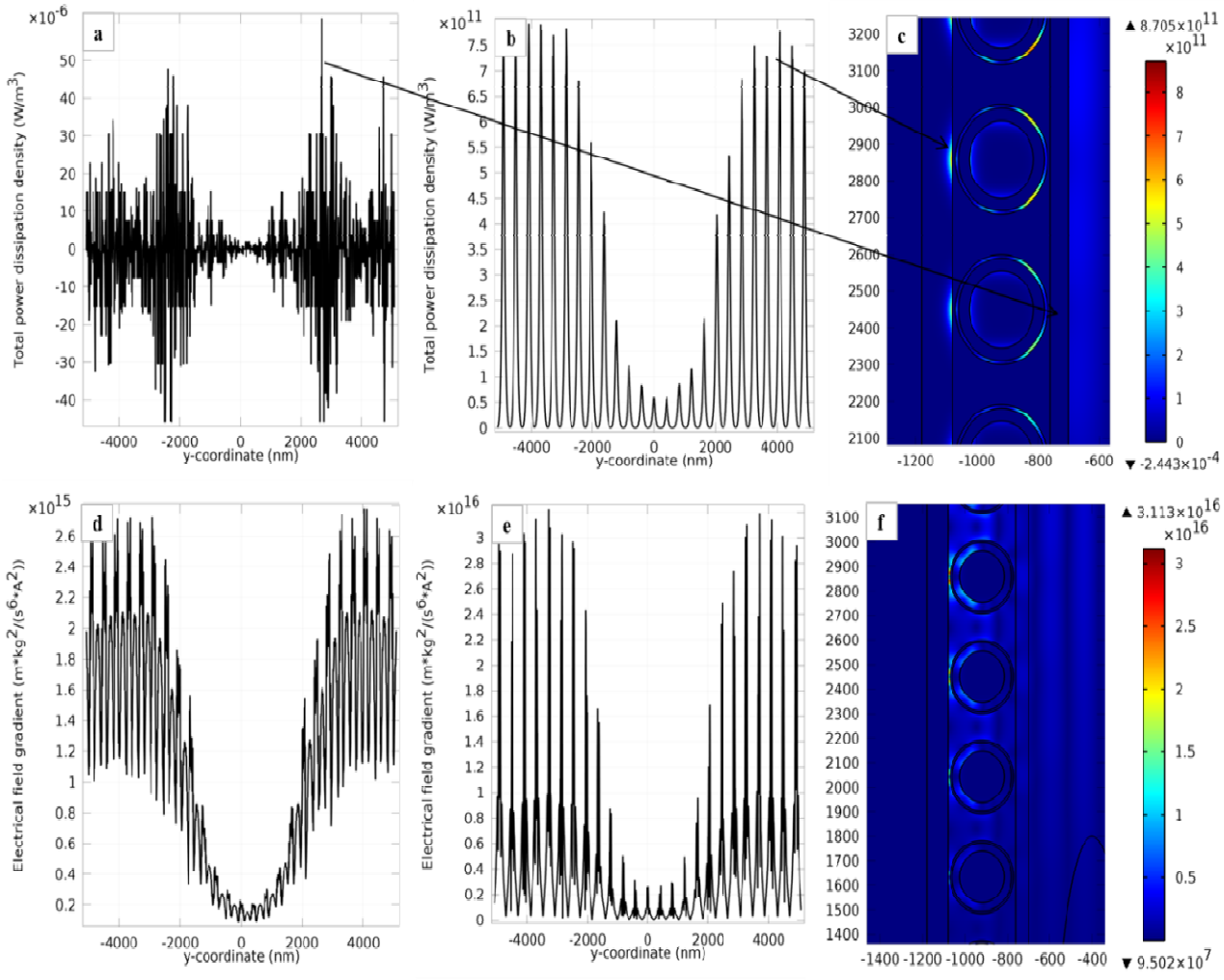

Figure. 4 Total power dissipation density (w/m^3) and electrical field gradient vs. y-coordinates; a) Total power dissipation density before nanosensor, b) Total power dissipation density after nanosensor, c) 2-D illustration of total power dissipation at around of NPs d) electric field gradient before nanosensor, e) electric field gradient after nanosensor, c) 2-D illustration of electric field gradient at around of NPs

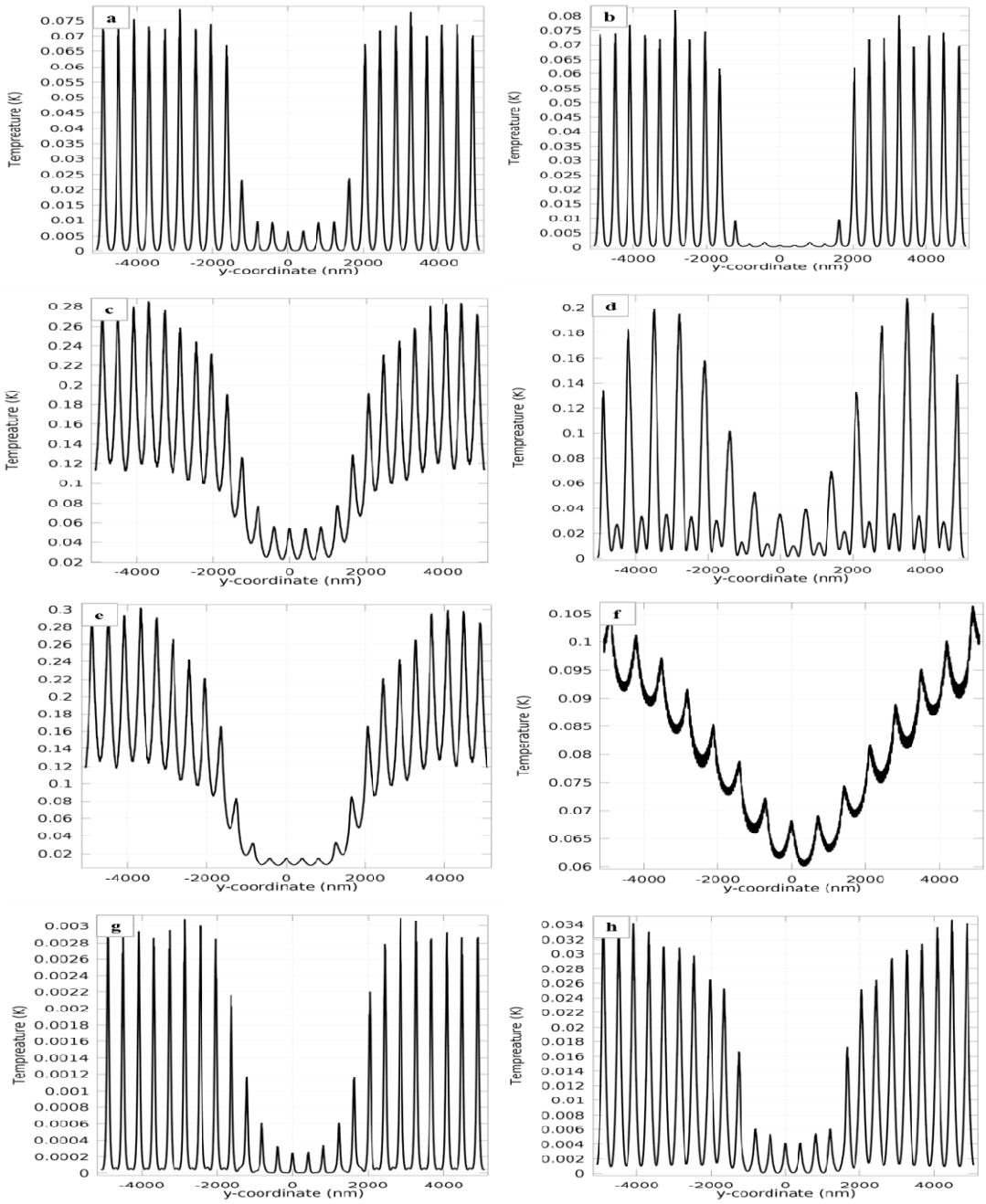

Figure. 5 Temperature (K) vs. y-coordinate (nm); a) non-Ideal state simulation (based on Table. 3); b) increasing of imaginary part of tumor indices (ntumor = 1.37+i0.9); c) changing of wavelength to 1550 nm; d) increasing of NPs distance from each other (from 110 nm to 400 nm); e) increasing of imaginary part of ntumor = 1.37+i0.9 and alteration of wavelength to 1550 nm; f) increasing of NPs distance from each other (from 110 nm to 400 nm) and alteration of wavelength to 6199 nm; g) alteration of medium materials: SiO_2 rather than silica aerogel; h) changing of core and second shell materials: Ag rather than Au.

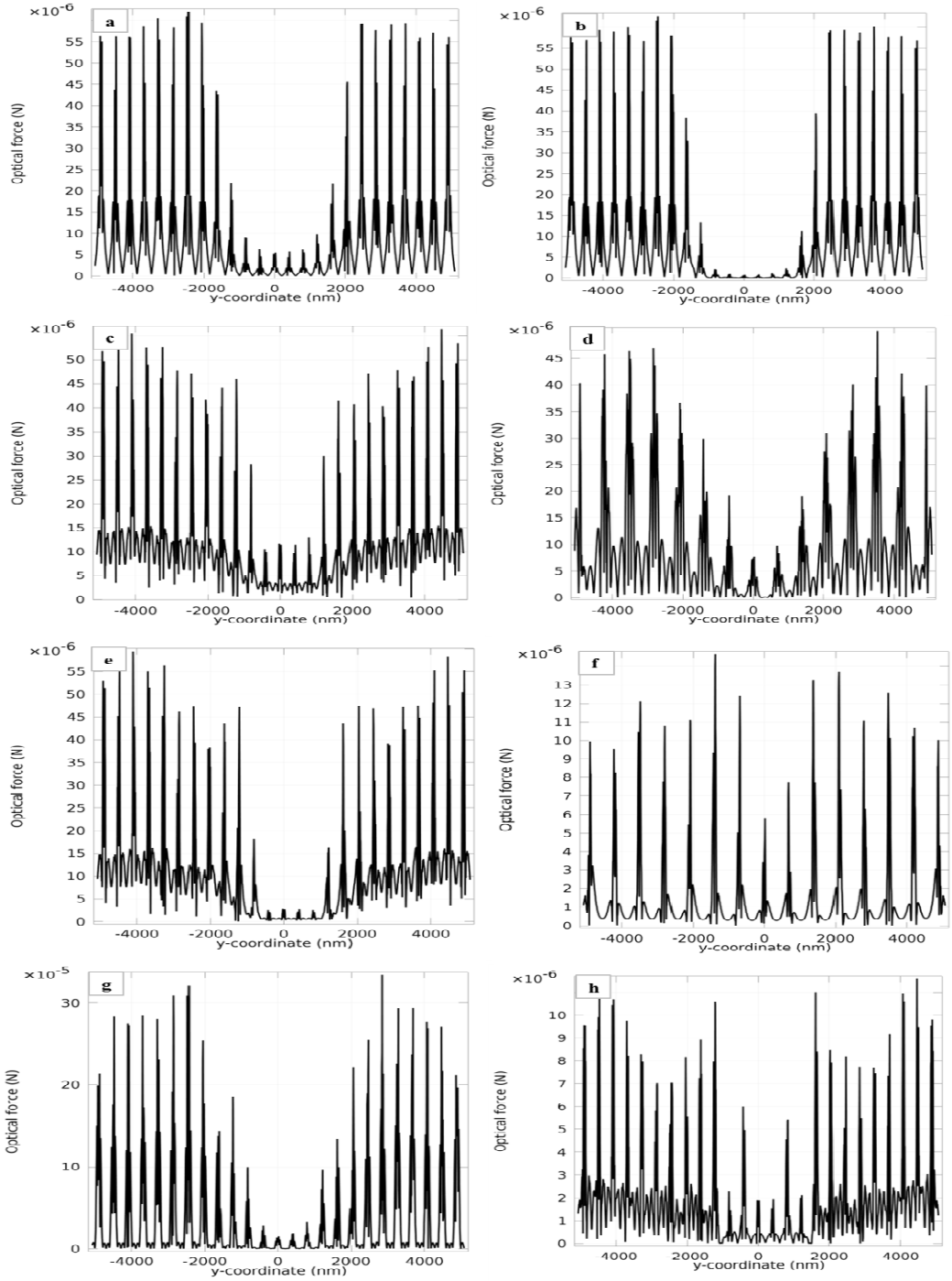

Figure. 6 Optical force (N) vs. y-coordinate (nm); a) non-Ideal state simulation (based on Table. 3); b) increasing of imaginary part of tumor indices (ntumor = 1.37+i0.9); c) changing of wavelength to 1550 nm; d) increasing of NPs distance from each other (from 110 nm to 400 nm); e) increasing of imaginary part of ntumor = 1.37+i0.9 and alteration of wavelength to 1550 nm; f) increasing of NPs distance from each other (from 110 nm to 400 nm) and alteration of wavelength to 6199 nm; g) alteration of medium materials: SiO_2 rather than silica aerogel; h) changing of core and second shell materials: Ag rather than Au.

$$(s.\nabla)L(r,s)=-(\mu_a+\mu_s)L(r,s)+(\mu_s/4\pi).\int_{4\pi} p(s,s').L(r,s')d\Omega \quad (1)$$

$$P_{delta-Eddington}(\cos\theta)=(1/4\pi).\{2f\delta(1-\cos\theta)+(1-f).(1+3g'.\cos\theta)\} \quad (2)$$

$$(s.\nabla)L(r,s)=-(\mu_t').L(r,s)+(\mu_s/4\pi).\int_{4\pi}(1+3g'(s,s')).L(r,s')d\Omega \quad (3)$$

$$L(r,s)=L_{col}(r,s)+L_d(r,s) \quad (4)$$

$$L_{col}(r,s)=(1-r_s).\pi F_0(r).\exp(-\mu_t'.z/\mu_0).\delta(\mu-\mu_0) \quad (5)$$

$$\begin{aligned}(s.\nabla)L_d(r,s)=&-(\mu_t').L_d(r,s)+\{(\mu_s'/4\pi).\int_{4\pi}(1+3g'(s,s')).L_d(r,s')d\Omega\}\\&+\{(1-r_s).\pi F_0(r).\exp(-\mu_t'.z/\mu_0).(\mu_s'/4\pi).(1+3g'\mu\mu_0)\}\end{aligned} \quad (6)$$

$$L_d(r,s)=(1/4\pi).\varphi_d(r)+(3/4\pi).F_d(r).s \quad (7)$$

$$\begin{aligned}(s.\nabla)\varphi_d(r)+3(s.\nabla)(F_d(r).s)=&-(\mu_a).\varphi_d(r)-3(\mu_t'-g\mu_s')(F_d(r).s)\\&+\{\mu_s'(1-r_s).\pi F_0(r).\exp(-\mu_t'.z/\mu_0).(1+3g'\mu\mu_0)\}\end{aligned} \quad (8)$$

$$\nabla^2\varphi_d(r)-3\mu_{tr}'\mu_a\varphi_d(r)=-3\{\mu_s'(1-r_s).\pi F_0(r).\exp(-\mu_t'.z/\mu_0).(\mu_{tr}'+g'\mu_t')\} \quad (9)$$

$$\langle F\rangle=(1/4).\mathrm{Re}(\alpha).\nabla|E|^2+(\kappa/2).\mathrm{Im}(\alpha).\mathrm{Re}(E^*\times B)+(1/2).\mathrm{Im}(\alpha).\mathrm{Im}[(E^*.\nabla).E] \quad (10)$$

$$\langle F\rangle=(1/2).\sum_i e_i.\mathrm{Re}[\alpha.E.(\partial E/\partial x_i)^*] \quad (11)$$

$$\langle F\rangle=\sum_i e_i.\mathrm{Re}(\alpha)(\partial|E|^2/\partial x_i)+(1/2)\sum_i e_i.\mathrm{Im}(\alpha).\mathrm{Im}[E^*.(\partial E/\partial x_i)] \quad (12)$$

$$\rho(r).c(r).\partial T(r,t)/\partial t=\nabla\kappa(r).\nabla T(r,t)+Q(r,t) \quad (13)$$

$$Q(r,t)=\langle j(r,t).E(r,t)\rangle_t \quad (14)$$

$$\Delta T(r)=V_{NPs}.Q(r)/4\pi.\kappa_0.r \quad (15)$$